Supporting Information

A novel electrocatalytic nanocomposite of reduced graphene oxide/silver nanocubes hybrid decorated imprinted polymer for ultra-trace sensing of Temozolomide

Purnendu Kumar Pathak, Anil Kumar and Bhim Bali Prasad*

Analytical Division, Department of Chemistry, Institute of Science, Banaras Hindu University, Varanasi - 221005, India

***Corresponding author:** E-mail: prof.bbpd@yahoo.com; Tel.: +91 9451954449; Fax: +91 542 2268127.

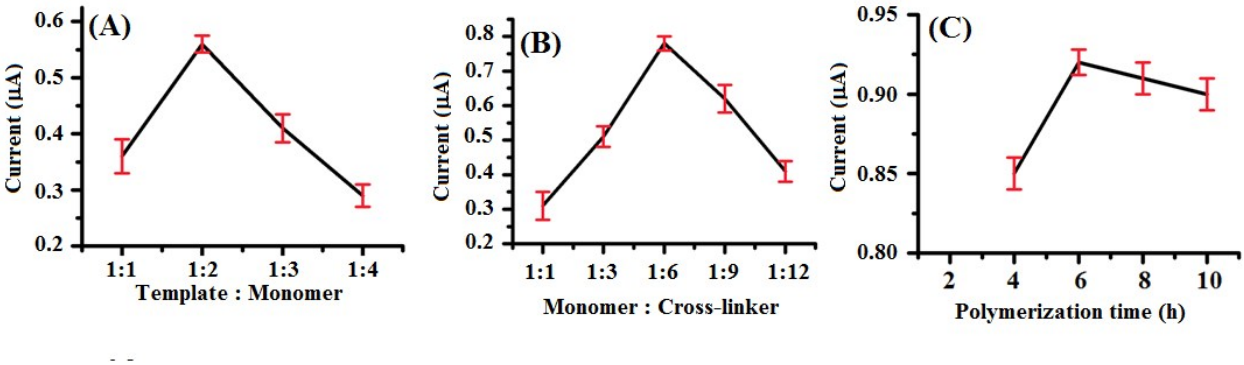

Fig. S1. Effect of template: monomer molar ratio (A), monomer: crosslinker molar ratio (B) and polymerization time (C) on DPASV response of TMZ.

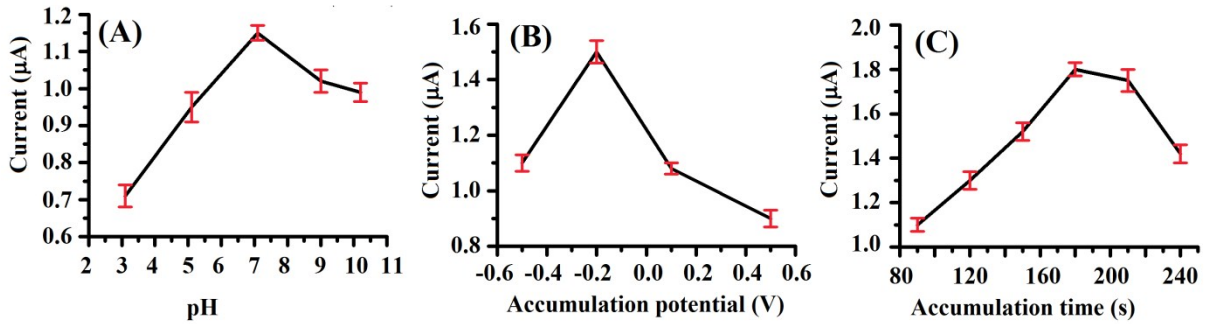

Fig. S2. Effect of analytical parameters: (A) pH of the supporting electrolyte, (B) accumulation potential, and (C) accumulation time on DPASV response of TMZ.

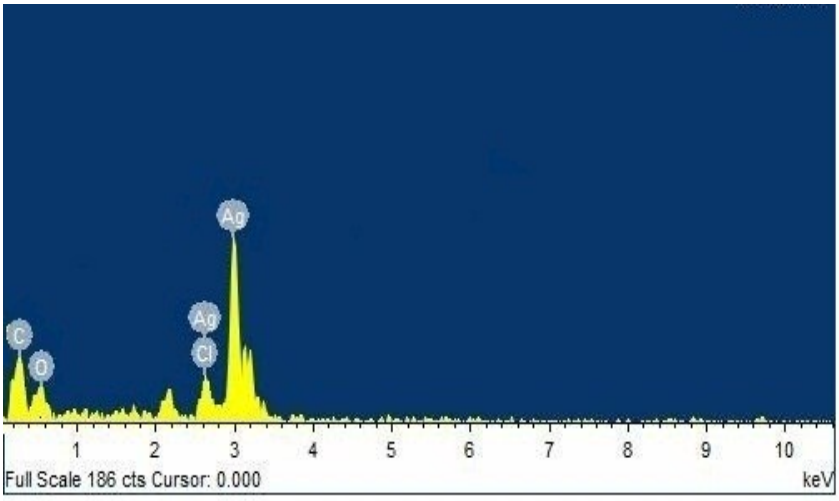

Fig. S3. EDS image of rGO/AgNC hybrid.

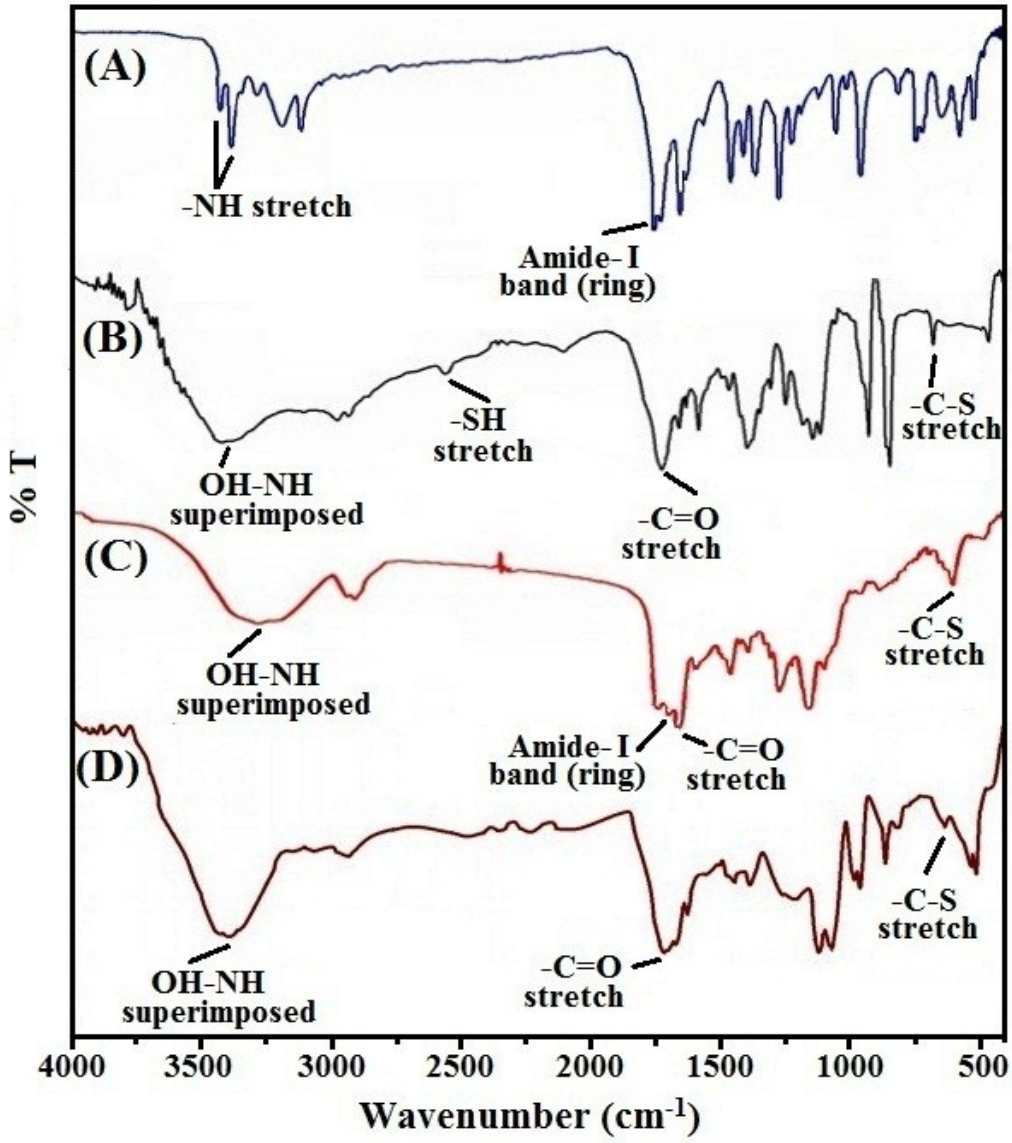

Fig. S4. FT-IR (KBr) spectra: (A) template, (B) monomer, (C) rGO/AgNC@MIP-adduct, and (D) rGO/AgNC@MIP.

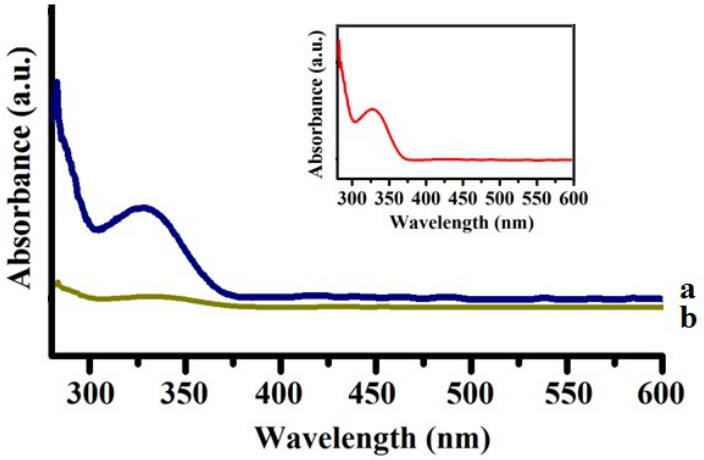

Fig. S5. UV-vis spectra of TMZ extract in methanol: water (4:1): (a) after 30 min and (b) after 40 min [inset shows UV-vis spectrum of standard TMZ solution (1 μg mL^{-1}) in methanol: water].

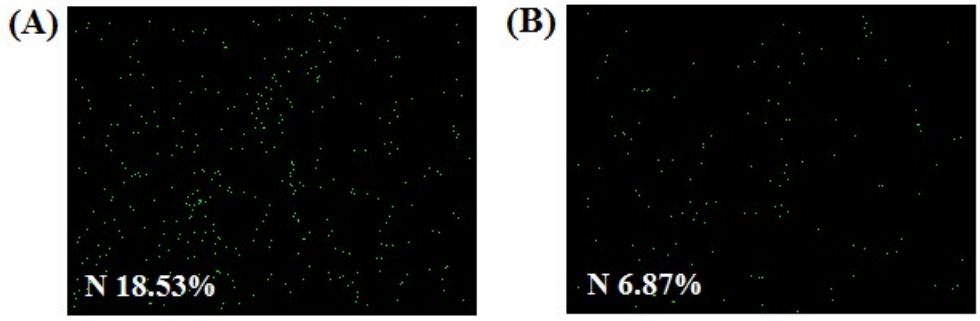

Fig. S6**.** Area mapping analysis for nitrogen element: (A) rGO/AgNC@MIP-adduct-SPCE and (B) rGO/AgNC@MIP-SPCE.

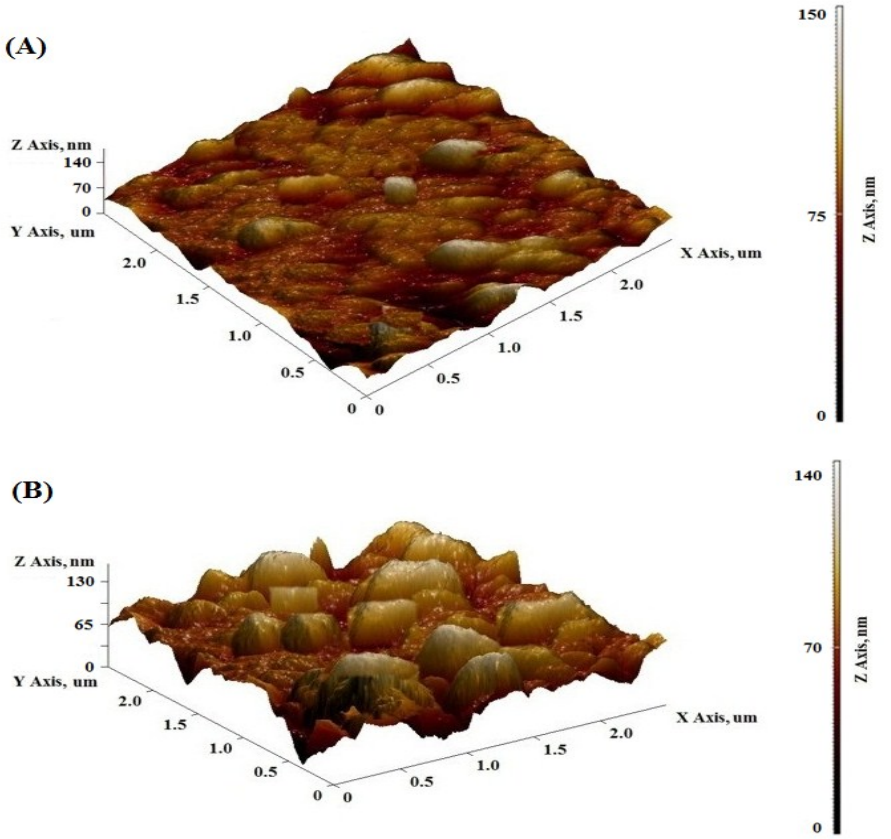

Fig. S7. AFM images: (A) rGO/AgNC@MIP-adduct and (B) rGO/AgNC@MIP modified SPCEs.

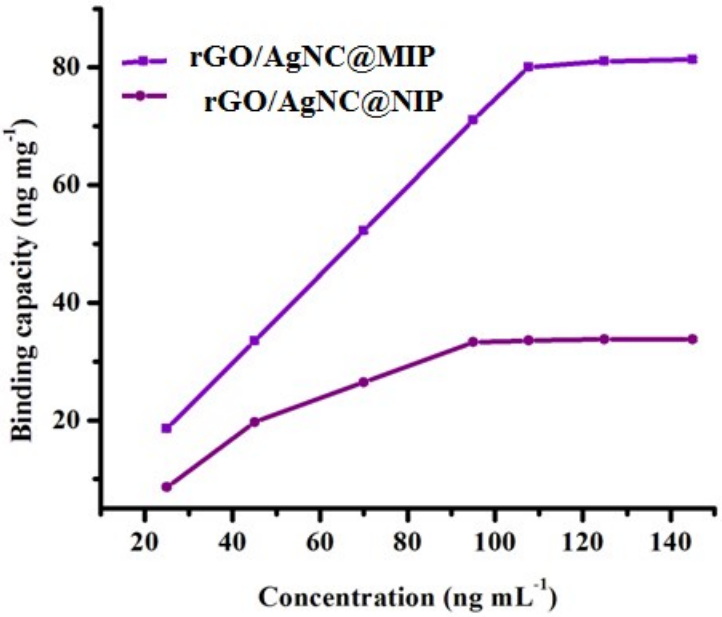

Fig. S8. Binding capacity of TMZ at rGO/AgNC@MIP and rGO/AgNC@NIP.

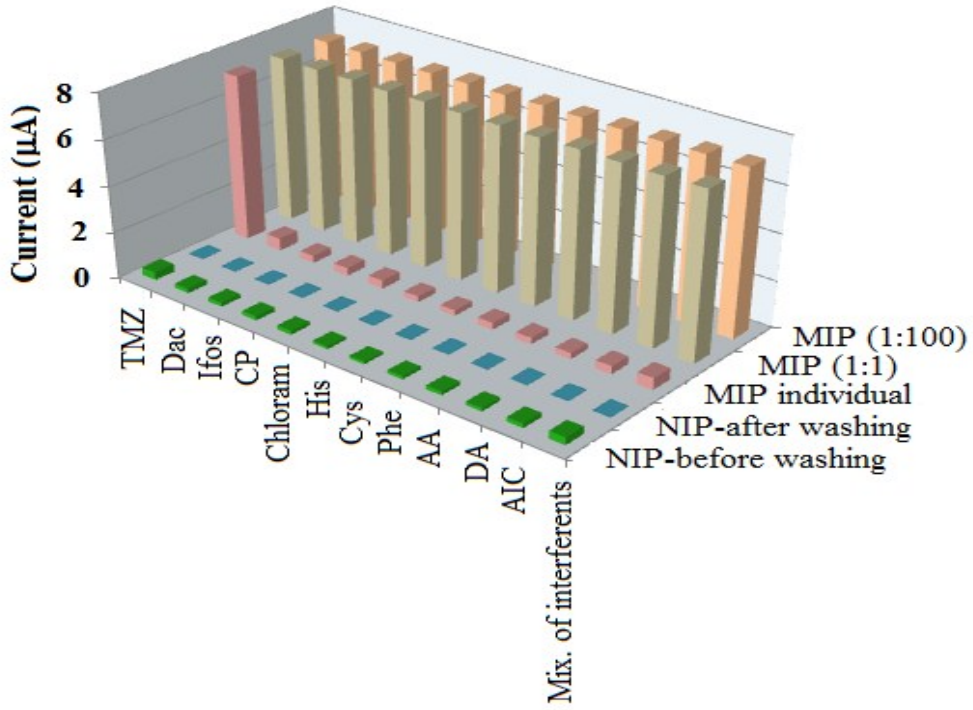

Fig. S9. DPASV response for TMZ and interferent(s) when studied either individually or in binary mixture (taken in 1:1 and 1:100 concentration ratio) on MIP and NIP modified rGO/AgNC-SPCEs.

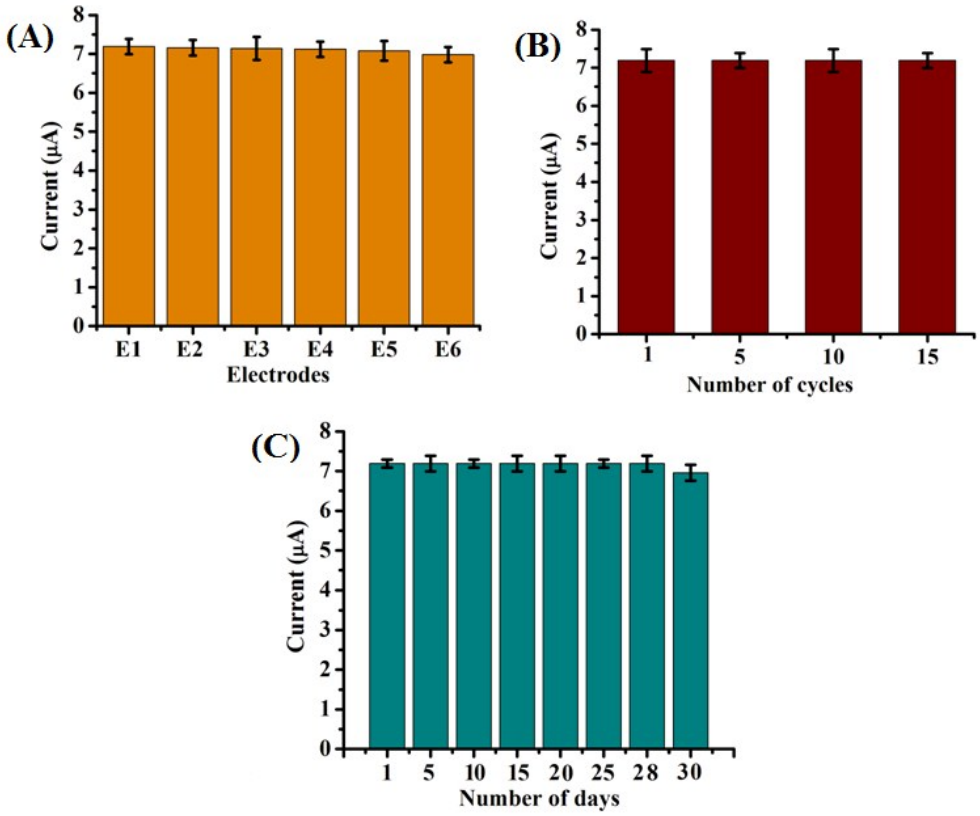

Fig. S10. (A) Electrode-to-electrode reproducibility, (B) regeneration ability of a single modified electrode, and (C) endurance of a single modified electrode (Electrode: rGO/AgNC@MIP-SPCE).

Table S1. Comparative studies of different electrodes.

Electrodes	**CV current (μA) for 0.1 mM of $[Fe(CN)_6]^{3-/4-}$**	**Peak separation (ΔE_p/mV)**	**A_{eff} (cm^2)**	**Roughness factor (R_f)**
Bare-SPCE	7.21	210	-	-
GO-SPCE	12.32	190	0.27	2.15
rGO/AgNC-SPCE	21.09	100	0.94	7.52
GO@MIP-SPCE	26.46	120	1.06	8.46
rGO/AgNC@MIP-SPCE	51.11	85	3.02	24.16

Table S2. Comparison of different methods of the determination of TMZ.

S.No.	Method	Range (ng mL^{-1})	*LOD* (ng mL^{-1})	Remarks	References
1	HPLC method	$(0.1\text{-}20.0) \times 10^3$	-	Poor sensitivity, expensive instrumentation, no interference study	[1]
2	HPLC with UV detection	$(0.1\text{-}20.0)\times10^3$	-	Poor sensitivity, expensive instrumentation, no interference study	[2]
3	HPLC-MS/MS	5-2000.0	-	Poor sensitivity, expensive instrumentation, complicated column preparation	[3]
4	RP-HPLC	$(10\text{-}100.0)\times10^3$	2.0×10^3	Poor sensitivity, expensive instrumentation, complicated, column preparation, no interference study	[4]
5	RP-HPLC with UV detection	$(20\text{-}60)\times10^3$	0.01×10^3	Poor sensitivity, expensive instrumentation, complicated column preparation, no interference study	[5]
6	UV spectrophotometric method	$(4\text{-}20.0) \times10^3$	-	Poor sensitivity, expensive instrumentation, no interference study,	[6]
7	UV spectroscopic method	$(4\text{-}18.0) \times10^3$	0.1×10^3	Poor sensitivity, expensive instrumentation, no interference study,	[7]
8	Pencil graphite electrodes	$(40\text{-}100.0)\times10^3$	6.1×10^3	Poor sensitivity, no interference study	[8]
9	Glassy carbon electrode	$(0.7\text{-}2.5)\times10^3$	0.2×10^3	Poor sensitivity, no interference study	[9]
10	rGO/AgNC@MIP-SPCE	1.1 – 144.2	0.16	Interference and real sample studies	Present work

Table S3. The selectivity coefficients (*k*), relative selective coefficients ($k^{'}$), and imprinting factor (*I.F.*) values obtained on rGO/AgNC@MIP and rGO/AgNC@NIP modified SPCEs.

Compound	**MIP**		**NIP**		***k´***	***I.F.***
	***I* (µA)**	***k***	***I* (µA)**	***k***		
TMZ	7.19	-	0.34	-	-	21.15
Dac	0.54	0.075	0.20	0.58	0.12	2.70
Ifos	0.32	0.044	0.17	0.50	0.08	1.88
Cycl	0.34	0.047	0.18	0.52	0.09	1.88
Chloram	0.36	0.050	0.16	0.47	0.10	2.25
His	0.25	0.034	0.12	0.35	0.090	2.08
Cys	0.24	0.033	0.11	0.32	0.10	2.18
Phe	0.30	0.042	0.14	0.41	0.10	2.14
AA	0.28	0.039	0.15	0.41	0.09	1.86
DA	0.26	0.036	0.15	0.41	0.08	1.73
AIC	0.35	0.049	0.19	0.55	0.08	1.84
Mix. of interferents	0.50	0.069	0.32	0.94	0.07	1.56

$$k = \frac{i_{interferent}}{i_{TMZ}},\ k^{'} = \frac{k_{MIP}}{k_{NIP}},\ I.F. = \frac{I_{MIP}}{I_{NIP}}$$

Supporting data Section

S.1

DPASV and CV runs were recorded on a portable potentiostat μ-Stat 200 (Drop Sens S.L. Oviedo, Spain) using rGO/AgNC@MIP-SPCE. This was connected via a USB connection to a computer installed with measurement software, Drop View (Drop Sens). Chronocoulometric measurements were performed with the same electrode assembly using an electrochemical analyzer (CH instruments USA, model 1200 A). FT-IR spectra were recorded on Varian 3100 FT-IR (USA) spectrometer, using KBr thin pellet containing the sample. The FT-Raman scattering measurements were carried out on a Renishaw in Via-plus micro-Raman system, at the room temperature, with 532 nm excitation wavelength. UV-vis analysis was performed on Varian Cary 100 Bio UV-visible spectrophotometer (USA). XRD patterns were obtained using ECO D8 model advance equipment (Bruker, Germany) using Cu Kα (1.5418 A^0) radiation. Morphological study of the rGO/AgNC hybrid was made using TEM [Technai-12FEI (Eindhoven, Netherlands)]. Surface morphologies of coatings were studied using SEM, Curl Zeiss, Supra-40 (Germany), and AFM [NT-MDT Co. (Russia) in semi-contact mode]. EDS was recorded on an Oxford instrument, X act (USA), attached to the Zeiss, Evo 18 research system, to study the elemental composition of rGO/AgNC hybrid. BET analysis was made using a micromeritics ASAP 2020 apparatus at the temperature of liquid nitrogen -195.56 ^{0}C for obtaining surface area of polymer motifs. Ultrathin coatings of GO and rGO/AgNC suspension and prepolymer solution over the SPCE surface were made using a standard spin-coater (ACE→ 200, Dong Ah Tech, Seoul, South Korea).

S.2

Cys (0.03 mol) and sodium nitrite (0.03 mol) were dissolved simultaneously in 30.0 mL potassium carbonate solution (5% v/v). Afterward, the mixture was ice cooled and MC (0.04 mol) was drop-wise added with vigorous stirring for 2 h. The pH of this solution was adjusted to 7.0 and then extracted with ethyl acetate. The aqueous phase was evaporated on a rotary evaporator at 100 ^{0}C. The crude MAC residue was crystallized in a mixed solvent, ethanol and ethyl acetate. [MAC, FT-IR (KBr, cm^{-1}): 3321 (OH-NH superimposed), 1717 (-C=O), 1656 (amide I), 1623 (amide II), 673 (C–S stretch) and 2552 (S–H stretch)].

S.3

To obtain the best performance of imprinted sensor, effects of different components of prepolymer mixture were investigated by altering each variable in turn while keeping the others constant. For this, template-monomer molar ratios (1:1, 1:2, 1:3, and 1:4) were varied in order to explore the stoichiometry of molecular complex that can lead to the maximum development of DPASV current response. In present instance, the maximum DPASV current response was obtained at 1:2 template-monomer ratio (Fig. S1A). The lower template-monomer ratio (say 1:1) in molecular complex exposed an inadequate number of binding sites that had a poor current response. On the other hand, the large template-monomer ratios (say 1:3, 1:4) had fewer numbers of binding sites exerting some non-specific binding in molecular complex. As a proof of this concept, the stoichiometry of molecular complex (template-monomer matrix) was calculated by an empirical equation:[10]

$$\frac{1}{i_p} = \frac{1}{i_p.max} + \frac{1}{i_p.max\,\beta\, C_t^m} \qquad (1)$$

where, i_p is the measured DPASV peak current, $i_{p\cdot max}$ the peak current when all template molecules formed complex with monomeric precursor, C_t is the concentration of template, m is the coordination number of the complex formed between template and monomer, and β is the stability constant. Substituting m = 1, 2, 3 and 4 in the above equation, the respective $1/i_p$ *vs* $1/C_t^m$ plots showed linearity with the coefficient of variation (R^2) 0.96, 0.99, 0.98 and 0.97, respectively for TMZ. Thus m = 2 could be accepted as a perfect straight line with R^2 = 0.99 for ascertaining template-monomer stoichiometry (1:2). Amount of cross-linker is another important parameters which affects the stability MIP networks. Accordingly, DPASV current was increased for the sensor fabricated with 1:6 molar ratios of monomer and EGDMA, owing to an improved stabilization of binding sites (Fig. S1B). Any increase of cross-linker amount higher than this ratio a decreased current response was obtained apparently due to highly cross-linked networking domain offering a poor access to the template. On the other hand, the lower amount of cross linker might not adequately stabilize the polymer matrix. The time required for the free radical polymerization ought to be optimized. In the present instance, the polymerization time of 6 h was found to be optimum to yield the maximum current response (Fig. S1C).

S.4

The pH of phosphate buffer solution (0.1M) had a major impact on the oxidation of TMZ (Fig. S2A). The DPASV peak current was gradually increased until it reached to a maximum at pH = 7.1 and then after decreased. At an optimized pH 7.1, MAC exists as a zwitter ionic form (*pKa* 4.23 and 10.23)[11] and TMZ in dicationic form (*pKa* 9).[9] Hence, at pH 7.1 TMZ molecules could electrostatically be bound to MIPs cavities. At pH >7.1, MAC exists as anionic form and TMZ in neutral form. However, at pH<7.1, both MAC as well as TMZ exists as cationic form. Hence, such electrostatic interactions are no longer feasible. Analyte accumulation at the electrode surface was optimum at a negative potential (E_{acc} = - 0.2 V); any potential higher and lower (< - 0.2V >) responded a diminishing current due to electrode-electrolyte repulsion and steric overcrowding amongst positively charged TMZ (under the influence of strong electrostatically driven accumulation), respectively (Fig. S2B). The optimum t_{acc} of TMZ was 180 s; thereafter a saturation of binding sites occurred in the sufficient time of deposition which restricted the current response (Fig. S2 C).

S.5

XRD pattern of graphite powder shows a sharp peak 2θ at 26.4^0 with a typical interlayer spacing of 0.34 nm (Fig. 1D, inset). Whereas after conversion of graphite to GO, a peak observed at 9.6^0 (Fig. 1D, curve a) can be ascribed to the characteristic diffraction peak of GO with d-spacing 0.86 nm. The higher d-spacing was obtained for GO (0.86 nm) in comparison to graphite powder (0.34 nm) this may be due the introduction of oxygenated functional groups on GO sheets. After the formation of rGO/AgNC hybrid, the diffraction peaks can be assigned for the cubic phase of Ag [37.7, 44.3, 64.4 and 77.3] and AgCl [27.6, 32.4, 46.1, 54.8 and 57.4] (Fig. 1D, curve b). No diffraction peak attributed to rGO is found because the anchored AgNC molecule disrupt the layered and ordered structure of rGO, and consequently leads to the disappearance of the refection peak.

S.6

Fig S4 shows the FT-IR (KBr) spectra of template (TMZ, curve A), monomer (MAC, curve B), rGO/AgNC@MIP-adduct (curve C), and rGO/AgNC@MIP (curve D). The analyte binding mechanism *via* electrostatic and hydrogen bonding interactions could tentatively be assigned

(Scheme 1) based on the respective downward shifts of the key bands participating in the complexation (self-assembly) process in between the monomer and the template. The characteristics bands of monomer [OH-NH superimposed (3319 cm^{-1}) and C=O stretch (1717 cm^{-1})] are shifted downwardly 3300 and 1673 cm^{-1}, upon complexation with template. Similarly, characteristics bands of template [-NH (3420, 3385 cm^{-1}) and amide-I (ring) (1755 cm^{-1})] are also shifted downward to 3300 and 1706 cm^{-1} owing to monomer-template hydrogen bondings and electrostatic interactions to form MIP-adduct. However, after template removal the bands corresponding to template are disappeared and monomer is reinstated at their original positions in MIP.

The complete extraction of template molecules from MIP-adduct was also confirmed by UV–vis spectrum. UV–vis spectrum of extract (methanol: water, 4:1 v/v), collected after 30 min, showed a characteristic peak for analyte at 327 nm. This eventually got vanished in the final extract collected in final extract after 40 min extraction (Fig. S5). To confirm this aspect, we have performed selected area mapping analysis during SEM investigation. Accordingly, the weight percentage of nitrogen was found to be 18.53% (calculated 19.31%,) for rGO/AgNC@MIP-adduct (Fig. S6A). Upon template retrieval from adduct, the weight percentages of nitrogen (observed 6.87%, calculated 7.14%) was decreased in rGO/AgNC@MIP (Fig. S6B). This indicates the complete retrieval of template molecules from rGO/AgNC@MIP-adduct.

S.7

Fig. S7 shows AFM images of rGO/AgNC@MIP-adduct and rGO/AgNC@MIP modified SPCEs. This suggested that surface-height (*Rz*) of rGO/AgNC@MIP layer to be 136.9 nm, arithmetic mean roughness (*Ra*) 12.6 nm, and root mean square roughness (*Rq*) 14.5 nm. On the other hand, the *Rz*, *Ra*, and *Rq* values for the rGO/AgNC@MIP-adduct were obtained to be 128.9, 11.9 and, 13.6 nm, respectively. The higher *Ra* and *Rq* value for MIP exhibited porous and rough surface than MIP-adduct. The high *Rz* value of MIP-adduct reflects the template implanted structure. An average thickness (t) of MIP layer on SPCE was calculated using the following equation:[12]

$$z(x,y) = s(x,y) + t + \Delta z(x,y) \qquad (2)$$

where *z(x,y)* is the surface-height (136.9 nm) of MIP, *s(x,y)* is the surface-height (5.12 nm) of the bare SPCE, *t* is the average thickness, and *Δz(x,y)* is the inherent roughness (*Rq* = 14.5 nm) of the MIP layer. The calculated value of mean thickness (*t*) of the rGO/AgNC@MIP modified SPCE coating was found to be 117.3 nm.

S.8

BET surface areas for rGO/AgNC@MIP and GO@MIP prepared in bulk are evaluated by the nitrogen adsorption technique. For this, 100 mg sample was placed in a sample holder, and degassed at 100 ^{0}C for 5 h. The specific surface area of rGO/AgNC@MIP (147.14 m^2 g^{-1}) was observed to be considerably higher than that of the GO@MIP (90.58 m^2 g^{-1}). Accordingly, rGO/AgNC@MIP nanocomposite had more porous texture than GO@MIP. Any calculation regarding surface area with the help of Impedance Spectroscopy exploiting the Nyquist plot appeared cumbersome presumably because of the hybrid nano-composition of rGO/AgNC surface.

S.9

Accordingly, the value of *D* of TMZ can be obtained by using integrated Cottrell equation[13] described as follows:

$$Q = 2nFAC(Dt)^{1/2}\pi^{-1/2} + Q_{ads} + Q_{dl} \quad (3)$$

$$Q_{ads} = nFA\Gamma^0 \quad (4)$$

where *A* is the electrochemical surface area of the electrode, *C* is the concentration (1.67×10^{-7} mol L^{-1}) of TMZ, Q_{dl} is the double layer charge, Q_{ads} is the faradic oxidative charge; other symbols have their usual meanings. Q_{dl} and total charge (Q_{dl} + Q_{ads}) were calculated from the respective intercepts of the Anson plots (Q *vs.* $t_{1/2}$) in the absence and the presence of TMZ at GO@MIP-SPCE and rGO/AgNC@MIP-SPCE. In order to obtained Γ^0, it is necessary to find number of electron '*n*' involved in oxidation of TMZ. The 'n' value is determined by the equation defining Nerstian adsorbent layer.[14]

$$I = \left[\frac{n^2F^2}{4RT}\right]\Gamma^0 Av \quad (5)$$

Accordingly, n is found to be 1.05. The Γ^0 is calculated to be 2.23×10^{-13} and 2.76×10^{-11} mol cm^{-2} for GO@MIP-SPCE and rGO/AgNC@MIP-SPCE, respectively. Therefore, the total electrode surface was covered by 2.36×10^{-13} mol (1.40×10^{11} molecules) and 8.33×10^{-11} mol (5.02×10^{13} molecules) of TMZ (each molecule occupied one molecular cavity) for GO@MIP-SPCE and rGO/AgNC@MIP-SPCE, respectively. From the slope of the Anson plot, '*D*' values calculated for TMZ are 3.54×10^{-5} and 9.04×10^{-4} cm^2 s^{-1} on GO@MIP-SPCE and rGO/AgNC@MIP-SPCE, respectively.

We have also calculated the standard heterogeneous rate constant (k) for TMZ oxidation at GO@MIP-SPCE and rGO/AgNC@MIP-SPCE surface, using Velasco equation:[15]

$$k = 1.11D^{1/2}(E_p - E_{p/2})^{-1/2}\nu^{1/2} \quad (6)$$

The estimated k values at GO@MIP and rGO/AgNC@MIP modified SPCEs are found to be 7.48×10^{-3} and 3.77×10^{-2} cm s^{-1}, respectively. The higher k value at rGO/AgNC@MIP-SPCE for TMZ indicated a fast kinetics involved without any interfacial barrier in the oxidation of TMZ than the GO@MIP-SPCE. It means that rGO/AgNC hybrid have effective mediation for electron transport.

S.10

Analyte (TMZ) adsorption onto rGO/AgNC@MIP-SPCE surface is specific and that can be determined by using Langmuir equation:[16]

$$\theta = \frac{bc}{1+bc} \quad (7)$$

where θ is the ratio of the Γ^0 at any concentration 'C' to its maximum surface coverage Γ^{max}. Eq. (7) can be rearranged as

$$\frac{C}{\Gamma^0} = \frac{1}{B_{ads}\,\Gamma^{max}} + \frac{C}{\Gamma^{max}} \quad (8)$$

where B_{ads} is the adsorption coefficient and Γ^{max} the maximum amount of analyte that can adsorb on the MIP surface. A linear relationship was obtained between C/Γ° and C, measured on rGO/AgNC@MIP-SPCE surface:

$$\frac{C}{\Gamma^0} = (0.17 \pm 0.01) \times 10^{11} c + (23.11 \pm 2.80),\ (R^2 = 0.98) \qquad (9)$$

Accordingly, the intercept (equivalent to slope / B_{ads}) of this equation gives an estimate of the adsorption coefficient (B_{ads}) equal to 7.15×10^8 L mol^{-1}. The Gibbs free energy change ($\Delta G = -RT\ ln\ B_{ads}$) due to analyte adsorption could be calculated as – 50.50 kJ mol^{-1}. The large negative value of ΔG_{ads} indicated spontaneous analyte adsorption onto the imprinted electrode surface.

S.11

To evaluate the electrode-to-electrode reproducibility of the proposed sensor, as many as six electrodes were prepared independently under identical preparation conditions, and examined the DPASV response of TMZ (30.4 ng mL^{-1}) (Fig. S11A). The relative standard deviations (*RSD*) in respective current of these solutions were maximally within 1.14%. This indicated an excellent reproducibility in making the electrodes. For the regeneration, the proposed sensor could be refreshed by extraction with methanol and water (4:1, v/v) simply applying mechanical stirring. Accordingly, the proposed sensor was able to maintain original sample behavior for many as many as 15 times with 1.68% *RSD*. In fact, current intensities were found to be decreased to 3.75% of the initial value, when the electrode was repeatedly used for more than 15 rebinding-extraction cycles (Fig. S11B). The long-term stability of the sensor, which depends on both the stability of the MIP-film and the activity of the TMZ, is also important to explore its practicability. The results show that the response of the sensor was decreased and maintained 96.8%, in comparison with the initial response, after four weeks duration (Fig. S11C).

References:

[1] H. Kim, P. Likhari, D. Parker, P. Statkevich, A. Marco, C.C. Lin and A.A. Nomeir, *J. Pharm. Biomed. Anal.*, 2001, **24**, 461–468.

[2] E. Gilant, M. Kaza, A. Szlagowska, K. Serafin-Byczak and P. J. Rudzki, *Acta Pol. Pharm. Ñ Drug Res*., 2012, **69**, 1347–1355.

[3] C.J. Peer, L. Ronner, L. Rodgers, C.M.L. McCully, K.E. Warren and W.D. Figg, *chromatography*, 2016, **3**, 1-10.

[4] A. Khan, S.S. Iman, M. Aqil, Y. Sultana, A. Ali and K. Khan, *Beni-Suef Univ. J. Basic Appl*. *Sci*., 2016, **5**, 402–408.

[5] B.M. Ishaq, K.V. Prakash and G. Krishnamohan, *Int. J. Chem. Sci*., 2013, **11**, 1055–1063.

[6] D.G. Sankar, P.V.M. Latha, B.A. Kumar and P.J. Babu, *Asian J. Chem*., 2007, **19**, 1605–1607.

[7] B.M. Ishaq, H.A. Ahad, S. Muneer, S. Parveen and B. Fahmida, *Int. Res. J. Pharm*., 2014, **5** 17–20.

[8] C. Altay, E. Eksin, G. Congur and A. Erdem, *Talanta*, 2015, **144**, 809–815.

[9] M. Ghalkhani, I.P.G. Fernandes, S.C.B. Oliveira, S. Shahrokhian and A.M. Oliveira-Brett, *Electroanalysis*, 2010, **22**, 2633–2640.

[10] X. Gao, *Handbook on the physics and chemistry of rare earth*, 1986, **8**, 63-201.

[11] T.A. Enache and A.M Oliveira-Brett, *Bioelectrochemistry*, 2011, **81**, 46–52.

[12] L.Y. Beaulieu, A.D. Rutenberg and J.R. Dahn, *Microsc. Microanal*., 2002, **8**, 422-428.

[13] A.J. Bard and L.R. Faulker*, Electrochemical Methods, second ed., Wiley, New York*, 2001.

[14] W. Hassen, C. Martelet, F. Davis, S. Higson, A. Abdelghani and S. Helali, *Sens. Actuators B: Chem*., 2007, **124**, 38-45.

[15] J.G. Velasco, *Electroanalysis*, 1997, **9**, 880-882.

[16] H. Ju and D. Leech, *J. Electroanal. Chem*., 2000, **484**, 150-156.

.